archives
of thermodynamics
Vol. **41**(2020), No. 1, 125–149
DOI: 10.24425/ather.2020.132952

Mathematical model and measurements of a combi-steamer condensation hood

MIESZKO TOKARSKI [a] *
ARKADIUSZ RYFA [a]
PIOTR BULIŃSKI [a]
MAREK ROJCZYK [a]
KRZYSZTOF ZIARKO [b]
ANDRZEJ J. NOWAK [a]

[a] Silesian University of Technology, Konarskiego 22, 44-100 Gliwice, Poland

[b] Retech Ltd., Wojska polskiego 6A, 39-300 Mielec, Poland

Abstract Combi-steamer condensation hoods are widely used in modern gastronomy. They condense steam produced by the combi-steamer and also filter solid particles, moisture, grease and smells. All these factors negatively affect the staff and dishes, so efficient work of the condensation hoods becomes important. A mathematical and experimental analysis of such a device is described in this paper. First a measurement methodology was designed and measurements of air humidity, temperature and mass flow rates were performed. The measurement procedure concerned dedicated a steam generator and combi-steamer. Next a mathematical model was developed. It was based on mass and energy balances of the condensation hood. The condensate flow rate turned out to be insufficient to fulfill the energy balance while measured directly. Hence, it was calculated from heater's power of the steam generator and the balance model was validated. The combi-steamer had an unknown output, so the condensate flow rate was provided by the balance model after its validation. A preliminary diagnosis of the device was carried out as well.

Keywords: Energy balance; Heat transfer; Heat exchanger; Condensation; Condensation hood

*Corresponding Author: Email: mieszko.tokarski@polsl.pl

Nomenclature

$\dot{H}$	–	enthalpy, kW
$\dot{m}$	–	mass flow rate, kg/s
$\dot{Q}$	–	rate of heat flow, kW
A	–	area, m^2
c	–	specific heat, kJ/(kg K)
h	–	specific enthalpy, kJ/kg
M	–	molar mass, kg/kmol
p	–	pressure, Pa
T	–	temperature, K
t	–	temperature, °C
w	–	humidity ratio, (mass of moisture)/(mass of dry air), kg/kg

Greek symbols

α	–	heat transfer coefficient, kW/(m^2K)
φ	–	relative humidity
ρ	–	density, kg/m^3
v	–	velocity, m/s

Subscripts

I-V	–	balance element
a	–	air
ad	–	additional
c	–	convection
ch	–	condensation hood
$cond$	–	condensate
da	–	dry air
fg	–	vaporization
ha	–	humid air
p	–	at constant pressure
ref	–	reference
s	–	saturation
$steam$	–	steam
v	–	moisture
$water$	–	water

1 Introduction

In contemporary gastronomy a modern foodservice equipment is more and more widely used. Combi-steamers are a key example as they are present in most restaurants as well as in cafeterias and supermarkets with their own bakeries. Combi-steamers significantly facilitate high-quality food preparation. Despite numerous advantages, they have one major drawback – produce a lot of steam. High moisture content could negatively affect the staff, customers and meals. When the use of stationary steam vents is not

possible, condensation hoods appear as a solution. The condensation hood captures the steam produced by the combi-steamer, condenses it and either returns the condensate back to the oven or sends it into the sewage [1,2].

The condensation hood is a subject of this paper. According to the best authors' knowledge, scientific publications analysing conjugate heat and mass transfer processes encountered in these devices are practically not available. However, component phenomena are typical and have already been investigated in other applications. Yet measurements of condensation hoods were not encountered by the authors in the literature.

The condensation hood consists of two parts: inlet – with filters and a fan that forces the air (from the environment) to flow through the device; and outlet – a heat exchanger (a condenser). At this point it should be stressed that in this heat exchanger the humid air from the environment (of low moisture content) works as a coolant while (most probably) mixture of the air and steam (of high moisture content) provided by the combi-steamer is cooled. As a result of this cooling, the high moisture content (the steam) eventually condenses. While pure steam condensation process is well described in most heat transfer related handbooks, in the presence of non-condensable gases (like in most cases – the air) the condensation process still needs further investigation. For instance, Su with use of commercial computational fluid dynamics (CFD) software and experimental data, investigated the impact of air content on steam condensation process over a vertical surface [3]. Fan developed a new empirical correlation for steam condensation in terms of pressure, air content and wall subcooling in a vertical smooth tube [4]. Abadi examined numerically steam condensation process inside a long, inclined, smooth tube at different saturation temperatures with assumption of the flow field being three-dimensional, unsteady and turbulent [5]. He also carried out a thorough literature review dedicated to condensation inside smooth tubes. Bian took up steam condensation process in tube bundles and performed numerical simulations on various cases. His research showed that tube bundles' configuration has a significant effect on the heat transfer coefficient in comparison to a single tube case [6]. O'Donovan investigated experimentally and mathematically the impact of pressure drop on steam condensation process in air-cooled tube bundles [7]. Due to a combination of frictional, momentum and gravitational effects, an excessive pressure drop may significantly affect the heat exchanger output. Tarasov carried out experimental studies of heat transfer during steam condensation on a bundle of slightly inclined tubes with

and without non-condensable gases at different steam pressures [8]. Fan in his work conducted experimental study of pure steam and air-steam mixture condensation on vertical corrugated and smooth tubes, respectively [9]. Those studies were carried out under different pressures and air content of the air-steam mixture.

Wide-ranging experimental and numerical studies regarding the steam condensation process in terms of numerous parameters prove that this phenomenon still needs investigation. Thus, design of efficient air-cooled condenser becomes challenging along with conducting reliable measurements.

The heat exchanger taken under consideration works with ambient humid air as a coolant. This type of heat exchangers is widely used in diverse applications and scales – from cooling electronic components [10] through refrigeration [11], as a car coolers [12] and air conditioning [13] to use in power plants and chemical industry [11,14]. Those solutions have one thing in common – the heat is transfered from hot fluid to an ambient air. Air flows on the outside of the pipes so dominant thermal resistance occurs on the air side [15]. For this reason pipes are frequently externally finned.

The typical configuration is different, when water is used as a coolant. Water flows inside the pipes while steam condenses on the outside of the pipes. As the heat transfer coefficient for water is higher than for the air there is no need for applying fins.

As for the case at hand, steam condenses outside the pipes and coolant (humid air) flows through the pipes. Hence, there is a need of reducing the thermal resistance inside the tubes. Therefore, internally finned pipes (with longitudinal fins) are used. This solution, although widely used in many industrial branches like power engineering [16–18], petroleum processing [18] or electronics [17–19], is not described in detail by standard general dimensionless correlations. Majority of works concerning internally finned tubes in various applications are focused on numerical [16–18] and/or experimental studies [20,16] in laminar [19] and/or turbulent flow regimes [16–18] in clearly specified, particular cases.

Investigation of a device equipped with non-standard heat exchanger with internally finned pipes, at least, requires the development of a mathematical model (system model, balance model). Such a model should be based on the mass and energy balances no matter if it is a car cooler [21], a refrigerator [22], a solar collector [23] or a heat exchanger itself [24]. In all these cases energy balance is crucial for the model to work properly. An experimental data is also necessary for validation [21,23].

Gathering experimental data from measurements can be problematic especially when numerous quantities have to be recorded simultaneously under unfavorable conditions. Hence, a selection of suitable probes becomes important. For example, a gas (air) flow rate measurement with the Pitot tube [25] (which is accurate and relatively simple in use) is very sensitive to installation, which has been investigated by Sun [26]. Additionally, each installed probe affects the flow of both heat and fluid, so complex measurements become even more challenging, when it comes to obtaining accurate results. Situation complicates, when the measurement of some quantity is not possible (due to unfavorable conditions or, simply, the lack of space for installing the probe). In order to compensate measurement errors, data reconciliation methods are developed and used. For example, Narasimhan developed an algorithm using iterative principal components analysis with a maximum likelihood estimation procedure for obtaining an estimate of the error covariance matrix together with the accurate process model [27]. Mandel described an alternative to the classical data reconciliation method based on likelihood function minimization with measurement errors distributions [28]. Narasimhan proposed two methods of data reconciliation, while the latter provides more accurate estimates of the uncertain model parameters [29].

In this paper a mathematical model of conjugate heat and mass transfer processes including condensation of water vapor taking place within the condensation hood is discussed in detail. This model is based on mass and energy balances of the condensation hood. It is also validated by measurements. To provide necessary experimental data to the balance model, mass flow rates were measured along with temperatures and air humidities. A steam generator was built in order to control the flow of the water vapor through the condensation hood. However, the condensation hood is dedicated to work with the oven, so the measurements had to be carried out on both the steam generator and the dedicated combi-steamer.

2 Condensation hood

Construction of the condensation hood can be divided into two parts – the first consists of front baffles, grease filters, front condensers and fan. Its main purpose is to clean the air and to pump it through the device. The second part is a heat exchanger with two bundles of pipes, steam inlets and air filter located at the outlet from the exchanger. Figure 1a presents sim-

plified scheme of the condensation hood with the most important elements highlighted. Detailed geometry of the device is shown in Fig. 1b.

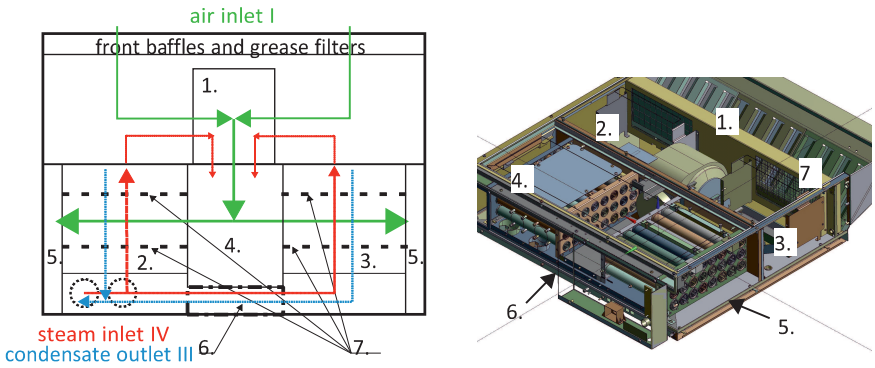

a) b)

Figure 1: Condensation hood: a) top schematic view, b) isometric view; 1 – fan, 2, 3 – bundles of pipes, 4 – air distribution chamber, 5 – peripheral air chambers, 6 – steam channel; 7 – steam baffles.

Front baffles are the first obstacle for solid particles suspended in the air. They are also used for aesthetic purposes. Grease filters are another replaceable part and prevent grease or sludge propagation from the environment into the device.

The condensate is removed from the device according to the thin dotted line in Fig. 1a. The fan 1, located in central part of the device, sucks the air (continuous line) from the environment and pulls it through an air distribution chamber 4 to pipes 2 and 3. It also sucks the remaining uncondensed steam (broken line) from the condenser and dilutes it in the air. Bundles of pipes 2 and 3 consist of 24 internally finned pipes each, which gives 48 pipes in total. The pipes are distributed uniformly in three rows along the whole length of the condenser. There are four vertical baffles 7 parallel to the pipes. They extend the distance to be covered by the steam and thus increase the performance of the device.

The air leaving the pipes flows through peripheral chambers 5 to the air outlet located above the heat exchanger equipped with an air filter (not shown in the figure).

The steam flows to the condensation hood through two inlets IV located in the left hand side pipe bundle 2. Then, some part of the steam flows through bundle 2, while the rest through the steam channel 6 to the bundle 3.

3 Mathematical model

Preliminary diagnosis of the condensation hood requires the mathematical model. This model is based on three balances written for a steady state: mass balance of dry air, moisture balance, and energy balance. It requires information about the velocities, temperatures and humidities at the inlets and outlets of the device.

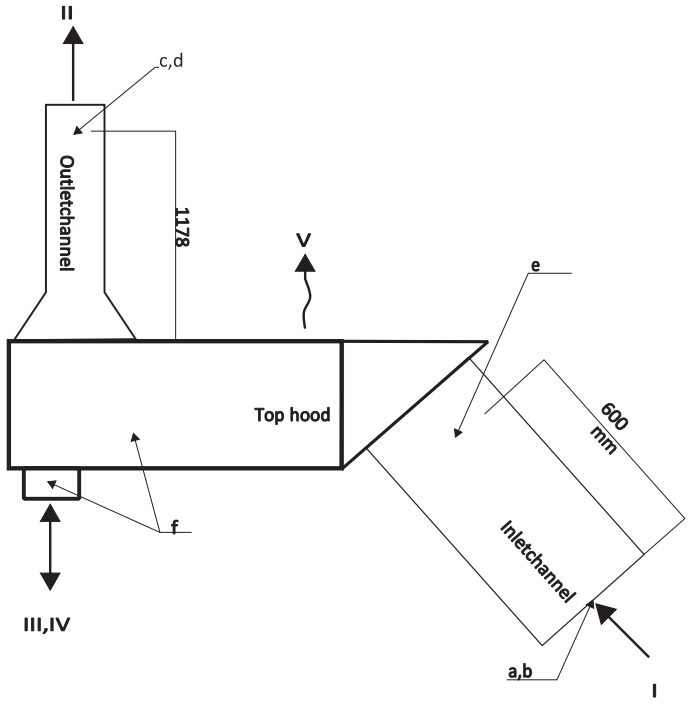

Figure 2: The hood's inlets, outlets and locations of measuring points.

Figure 2 presents the hood's inlets, outlets and measuring points I–V of the following quantities:

I – air inlet: temperature, relative humidity and velocity,

II – air outlet: temperature, relative humidity and velocity,

III – condensate outlet: mass and time,

IV – steam inlet: temperature,

V – heat losses: temperature of the housing.

3.1 Mass balance of dry air

According to the principle of mass conservation, in open systems in a steady state the total amount of matter that inflows and outflows of the system should be equal to each other. In fact, however, there is always some uncertainty resulting from the measurement error. Hence, the mass balance of dry air takes the form

$$\dot{m}_{da,I} = \dot{m}_{da,II} + \Delta\dot{m}_{da} \ , \tag{1}$$

where $\dot{m}_{da,I}$ and $\dot{m}_{da,II}$ are mass flow rates of dry air at air inlet and outlet respectively, $\Delta\dot{m}_{da}$ is balance of dry air inconsistency.

In fact, direct measurements bring information about mass flow rate of humid air and obtained results need to be converted considering air humidity ratio [15]. To do so, the humidity ratio is needed

$$\dot{m}_{da,I} = \dot{m}_{ha,I}\frac{1}{(1+w_I)} \ , \tag{2}$$

where $\dot{m}_{ha,I}$ is the mass flow rate of humid air at point air inlet (I), w_I is the humidity ratio, (mass of moisture)/(mass of dry air). The mass flow rate of humid air can be expressed as

$$\dot{m}_{ha,I} = A_I\overline{\nu}_I\rho_{ha,I} \ , \tag{3}$$

where A_I is a cross-sectional area at the air inlet, $\overline{\nu}_I$ is average air velocity, and $\rho_{ha,I}$ is air density.

The humidity ratio in Eq.(2) is defined (according to [15]) as

$$w_I = \frac{\varphi_I p_s}{p_{ref} - \varphi_I p_s}\frac{M_{h2o}}{M_a} \ , \tag{4}$$

where φ_I stands for relative humidity, p_s is the saturation pressure of water at temperature at air inlet (point I), p_{ref} is reference pressure (here atmospheric pressure), M_{h20} is the molar mass of water, and M_a is molar mass of dry air. The same equations apply to the outlet air (point II) as well.

3.2 Moisture balance

The principle of mass conservation applies to the moisture balance as well. The balance of the condensation hood consists of the following elements:

$$\dot{m}_{v,I} + \dot{m}_{steam,IV} = \dot{m}_{v,II} + \dot{m}_{cond,III} + \dot{m}_{cond,III,ad} \ , \tag{5}$$

where $\dot{m}_{v,I}$ is the moisture flow rate at the inlet, $\dot{m}_{steam,IV}$ is steam input, $\dot{m}_{v,II}$ is moisture flow rate at the outlet, $\dot{m}_{cond,III}$ is the condensate flow rate, and $\dot{m}_{cond,III,ad}$ stands for an additional condensate flow rate closing the balance.

Moisture flow rates at the inlet I and outlet II of the condensation hood are defined as follows:

$$\dot{m}_{v,I} = \dot{m}_{da,I} w_I \ . \tag{6}$$

3.3 Energy balance

The energy balance, similar to the mass balances, has been extended by the energy balance inconsistency, $\Delta\dot{H}$. Eventually, energy balance of the condensation hood takes the form

$$\dot{H}_I \ + \ \dot{H}_{IV} \ = \ \dot{H}_{II} \ + \ \dot{H}_{III} \ + \ \dot{Q}_V \ + \ \triangle\dot{H} \ , \tag{7}$$

where $\dot{H}_I$ stands for the air enthalpy at the inlet, $\dot{H}_{IV}$ is steam enthalpy, $\dot{H}_{II}$ is air enthalpy at the outlet, $\dot{H}_{III}$ is condensate enthalpy, $\dot{Q}_V$ stands for heat losses, and $\Delta\dot{H}$ is energy balance inconsistency. This last quantity is in some sense a measure of measurement accuracy of all thermal quantities involved in the energy balance.

Air enthalpies are calculated as follows:

$$\dot{H}_I = \dot{m}_{da,I} c_{p,a} \left\{ (T_{a,I} - T_{ref}) + w_I \ \left[h_{fg} + c_{p,steam} (T_{a,I} - T_{ref}) \right] \right\} \ , \tag{8}$$

where $c_{p,a}$ stands for the air specific heat, $T_{a,I}$ is temperature of air, T_{ref} is reference temperature, h_{fg} stands for enthalpy of vaporization (latent heat), and $c_{p,steam}$ is specific heat of steam.

Enthalpy of the steam is calculated as a product of steam mass flow rate and specific enthalpy

$$\dot{H}_{IV} = \ \dot{m}_{steam,IV} h_{steam} \ , \tag{9}$$

where h_{steam} stands for the specific enthalpy of the steam.

The enthalpy of the condensate is relatively low in comparison to other elements of the energy balance, but it has still been taken into account and derived as follows:

$$\dot{H}_{III} = \dot{m}_{cond,III} c_{p,water} (T_{cond,III} - T_{ref}) \ , \tag{10}$$

where $c_{p,water}$ stands for the specific heat of water, and $T_{cond,III}$ is the condensate temperature.

Heat losses are the last element of the balance. Convective heat transfer is dominant (the condensation hood housing has a low temperature of 30–50 °C in the region of heat exchanger) but also negligibly small

$$\dot{Q}_V = \alpha_c A_{ch} \left(\overline{T}_{ch,V} - T_{ref} \right) , \tag{11}$$

where α_c is an average convection heat transfer coefficient, A_{ch} is a heat transfer surface area, and $\overline{T}_{ch,V}$ is an average temperature of the heat transfer surface.

3.4 Condensation efficiency

The main function of the condensation hood is steam condensation. Hence, the condensation efficiency becomes the most important parameter calculated as follows:

$$\eta = \frac{\dot{m}_{cond,III}}{\dot{m}_{steam}} 100\% . \tag{12}$$

4 Measurement methodology

Good quality measurements are necessary to the verify mathematical model. Thus, it becomes crucial to prepare an appropriate experimental rig along with measurement procedure including measured values and measurement devices (also taking into account their number, location, accuracy, range and measurement conditions).

The following probes were used during the measurements:

(a) Omniport30 Logprobe 16 – temperature (-20–70 °C ±0.5°C), pressure (900–1100 hPa ±0.5 hPa), realtive humidity (0–100% ±2% for 0–90% and ±3% for 90–100%).

(b) Omniport30 Logprobe 65 – velocity (0–20 m/s ±0.2 m/s), temperature (0–50°C ±1°C).

(c) Delta Ohm HD29371TC.../HD29V371TC – velocity (0.05–20 m/s ±0,7 m/s+3% of the value), temperature (-10–60°C ±0.3°C), relative humidity (0–100% ±1.5% for 10–90% and ±2% for the remaining range).

(d) Dwyer 167-12" Pitot tubes with Dwyer Magnesense II Differential Pressure Transmitter – velocity (0–20 m/s ±1% up to 50 Pa).

(e) Dwyer 160-36" Pitot tubes with Dwyer Magnesense II Differential Pressure Transmitter – velocity (0–20 m/s ±1% up to 50 Pa).

(f) Thermocouples type K – temperature (-60–375°C ±0.1°C).

Letters a to f in Fig. 2 denote probes described above, while arrows indicate their approximate locations.

Readings from all the sensors except for (a) and (b) were recorded by a Brainchild PR20 signal recorder. To properly measure the velocity at the air inlet and outlet, additional channels were introduced. They also allowed for equalization of the velocity profile at the outlet from the device. The measurement probes were precisely mounted in these channels. The inlet channel was a simple cuboid with a constant rectangular cross-section along its entire length. It was well matched with the condensation hood to eliminate air leakage.

Two Pitot tubes (e) were placed in the geometrical centers of both halves of the inlet channel cross-section 0.6 m away from the inlet to the channel. Additionally, ambient pressure, temperature and relative humidity were measured and allowed for determining of the humidity ratio at point I with the use of probe (a). The velocity profile at this point was verified with the use of probe (b) by manual measurements.

As the velocity at the outlet was found to be low (less than 1 m/s) and highly non-uniform, it has been decided to prepare a channel with extension having a smaller cross-section. Hence the outlet channel had a trapezoidal constriction and a straight rectangular part. The cross-sectional area of the extension was reduced four times relative to the outlet of the condensation hood itself. Despite this effort the velocity profile at the condensation hood air outlet was still non-uniform. Therefore velocity measurements have been conducted with the use of Pitot tube (d) in 25 points throughout the cross-section according to the log-Chebyshev method described in [30] (used during traversing a duct to determine the average air velocity) and an average value has been compared to the readings from the stationary sensors mounted in the channel. The average velocity from the log-Chebyshev method was close to the one measured by probe (c), which proved that the non-uniform velocity profile did not affect the results in this case. The length of this channel was limited by the available height of the laboratory. Figure 2 presents the location of point II with sensors (c) and (d) while Fig. 3 shows their actual placement inside the channel. Further reducing the cross-sectional area of the outlet channel was not possible due to dimensions of the sensors (c) – the distance between measurement

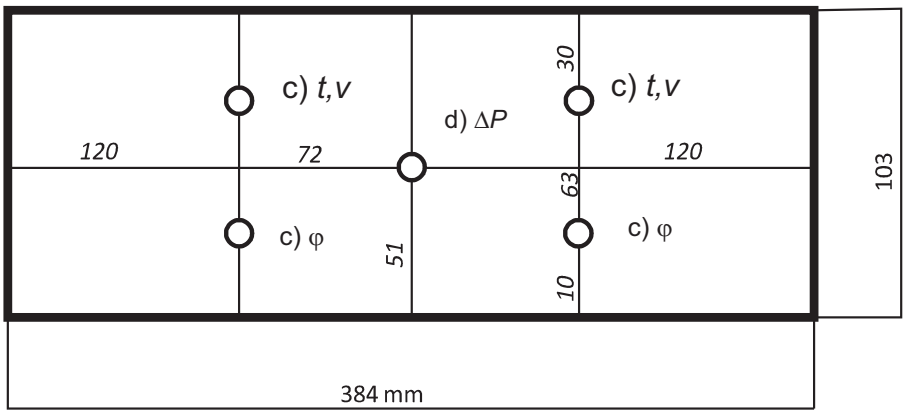

Figure 3: Outlet channel cross-section with location of measurement points: t – temperature; v – velocity; φ – relative humidity; ΔP – velocity (Pitot tube).

points of temperature/velocity and relative humidity. For this reason, an additional velocity measurement was carried out by Pitot tube (d) inserted to the center of the channel.

The condensation hood has been examined in three cases of cooperation with:

Case A: A low-powered steam generator (3.4 kW).

Case B: A high-powered steam generator (27 kW).

Case C: A combi-steamer.

Preliminary measurements showed that the condensate flow rate is not sufficient to fully satisfy the energy balance (Eq. (7)). Additionally the condensation hood works with no natural slope, so gathering of the condensate may be problematic. To improve this situation we prepared a dedicated scaffolding presented in Fig. 4. This solution allowed for easy condensate gathering through gravitational forces. Due to an increased distance between the devices, use of the specially designed fittings (SDF) became necessary. The SDF branched into two transparent pipes (see Fig. 5) converging in upper part. Segment a–f was used for condensate gathering, while b–a to provide the condensation hood with steam.

Steam generators (Case A and Case B) are schematically presented in Fig. 5. Both of them consist of a water tank b and an electric immersion heater d. The condensation hood a is placed on the scaffolding (not shown in this figure) providing a global slope towards the bowl f where the condensate is gathered. The device a is connected with the water tank b by

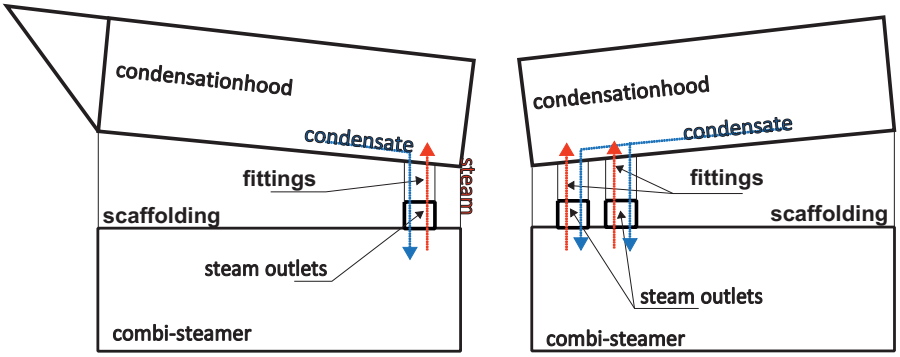

Figure 4: Scheme of the condensation hood position relative to the combi-steamer with scaffolding; outlet channel not included: left-hand side – side view, right-hand side – rear view.

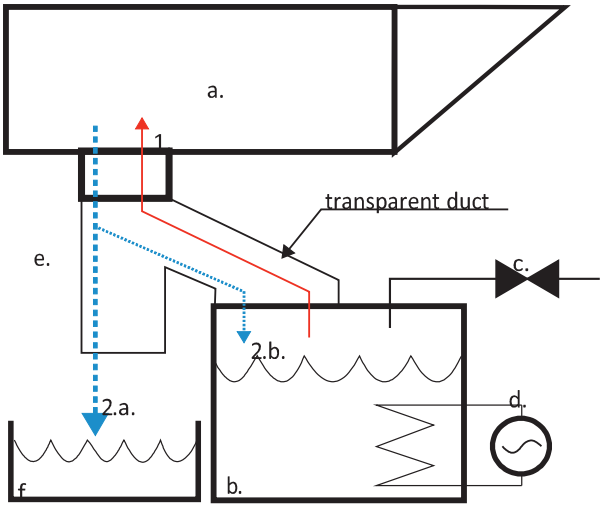

Figure 5: Scheme of the steam generators: a – condensation hood; b – water tank (or combi-steamer); c – water supply valve; d – electric immersion heater; e – SDF; f – condensate container; 1 – steam; 2 – condensate.

SDF e. Additionally, the low-powered steam generator was equipped with a hot water supply valve c to extend the measurement time. Low-powered steam generator (Case A) provided the known and constant over time mass flow rate of the steam delivered to the condensation hood. The steam flow rate was determined twofold: based on the mass of evaporated water in a specified period of time and from the heater power. This allowed for de-

termination of the expected condensate flow rate and for comparison with the actually measured one. Secondly, the maximum time of measurements was not limited, so a thermal quasi steady state was achieved improving quality and reliability of the measurements.

In the case of a high power steam generator (case B), the possible time of measurement was a main limitation. Namely, the volume of the water tank (about 0.006 m^3) allowed for about 10–15 min. of measurement, i.e. until most of water evaporated. However, for such high heating power, i.e. 27 kW, a steady state was achieved much quicker than in the low-powered steam generator as well as in the combi-steamer case.

The steam generators were used to simulate known input into the condensation-hood. The mass flow of steam was selected in a typical operating range of the condensation hood (Case A). It also allowed for verification of the chosen measurement methodology. Second experiment (Case B) was conducted to assess the maximum condensation capacity of the device. Here the amount of generated steam greatly exceeded typical conditions. The same scheme (Fig. 5) applies to the combi-steamer (Case C) as well. However, the heater power along with the water supply flow rate are unknown in Case C.

Originally the condensation hood returns the condensate back to the combi-steamer or to the water tank (see Fig. 2 point III). The remaining water evaporates and is then released to the environment II with humid air. In the case of steam generators, the problem of condensate gathering was solved by the known heater power. In addition, the steam enthalpy can be calculated according to Eq. (9). The condensation hood is supplied with a mixture of steam and air by the combi-steamer, what makes any reliable and non-invasive measurement of the flow rate at point IV practically impossible. The temperature at the steam inlets was measured with the use of thermocouples f in Fig. 2.

Heat losses were the last determined element of the energy balance taken into account in the mathematical model; in Fig. 2 denoted as V. Due to a relatively low temperature of the condensation hood sheathing, only convection has been considered. As expected, the obtained heat losses were negligible (less than 1% of the heater power).

Additional 8 thermocouples f were placed in the internal heat exchangers as presented in Fig. 6. For more information about the heat exchangers, please refer to Section 2 Fig. 1. Four air side thermocouples (outside the outline of the exchangers) were doubled located one above the other. Re-

maining 4 sensors were mounted inside the exchangers shells, which allowed for heat load examination of both pipe bundles and later for validation of the numerical model. This is, however, a subject of separate study.

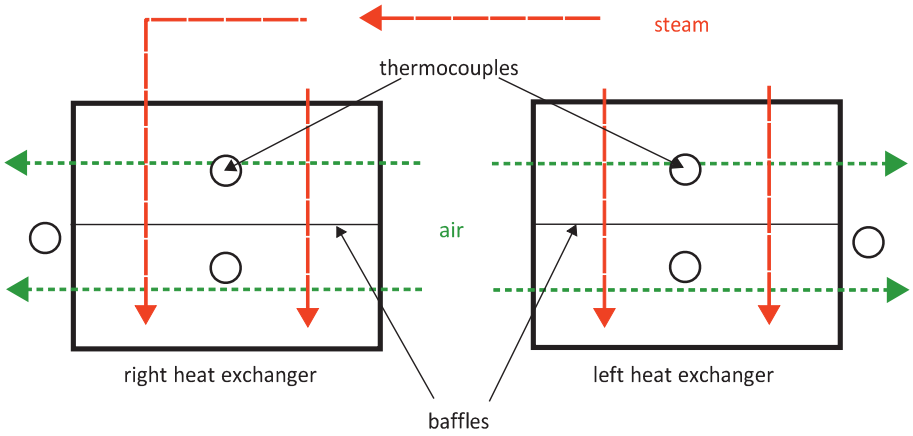

Figure 6: Scheme of the condensation hood heat exchangers – top. Two baffles included.

During the first few series, additional manual measurements of inlet and outlet velocity profiles have been carried out with the use of probe b. Their results proved that those profiles are constant for each gear of the fan regardless of the condensation hood workload. The obtained air mass flow rates correspond well with the results provided by the Pitot tubes despite the outlet profile non-uniformity.

In the case of low-powered steam generator A, the measurement procedure can be presented as follows:

(i) fan gear set up,

(ii) ambient conditions measurement,

(iii) filling the water tank and setting the heater power at 3.4 kW,

(iv) start of the measurement after steady-state is reached,

(v) start of the temperature/velocity/humidity recording,

(vi) and of the measurement,

(vii) additional ambient conditions measurement.

Measurement procedure in the case of high-powered steam generator B is quite similar to that of case A apart from points iii and iv, where the

heater power is set at 27 kW and the measurement begins after the water is boiled.

The measurement procedure is common for each combi-steamer set up, including a chosen operating mode, temperature and cooking function (if available). Several main steps of the procedure can be distinguished:

(i) fan gear set up,

(ii) combi-steamer programme set up,

(iii) ambient conditions measurement,

(iv) start of the condensate mass flow measurement as soon as a thermal quasi steady-state is reached. Start of the temperature/velocity/humidity recording,

(v) ambient conditions measurement,

(vi) end of the measurement.

5 Selected main results of measurements

The measurements have been carried out in three cases described in Section 4: A – low-powered steam generator; B – high-powered steam generator and C – the combi-steamer. According to the above, the measurements are labeled with letters A, B and C, respectively. Numbers standing by the letters denote subsequent measurement series. Two additional parameters are involved: CT (crisp & tasty) – a parameter responsible for additional food drying; HP – Humidity Pro – a parameter responsible for additional humidity increase in the working chamber. The full list of examined operating modes is as follows:

A1-2 – steam generator, 3.4 kW,
B1-2 – steam generator, 27 kW,
C1 – combi-steamer, convection mode, 150 °C, CT1,
C2 – combi-steamer, steam mode, 100 °C,
C3 – combi-steamer, convection mode, 250 °C, CT1,
C4 – combi-steamer, combi-steam mode, 250 °C, HP3,
C5 – combi-steamer, combi-steam mode, 250 °C, HP5.

Series C1 and C3 were investigated with CT parameter set to 1 out of 5 in order to minimize its impact on steam production. The higher is CT, the lower steam is being produced. Series C4 and C5 were examined with HP parameter set to 3 and 5 respectively in 5-grade scale, which means that

a medium and the highest available HP values were used in experiments. What is more, all the operating modes were set to their maximal temperature, so the condensation hood could be examined in the most demanding conditions.

Table 1: Steam generators – measurements.

Steam generator	3.4 kW		27 kW	
Symbol	A1**	A1	B1	B2
t_I, °C	24.9	24.9	32.8	26.0
φ_I, %	42	42	32	28
p_I*, kPa	98.71	98.71	100.23	100.23
t_{II}, °C	38.3	38.3	65.3	63.0
φ_{II}, %	21	21	33	28
p_{II}, Pa	14	14	13	16
$\dot{m}_{steam,IV}$, g/s	1.38	1.36	11.49	11.50
$\dot{m}_{cond,III}$, g/s	1.25	1.25	2.91	4.15
Gear	1	1	1	2

*reference pressure
**steam mass flow rate $\dot{m}_{steam,IV}$ calculated from water gauge

Sample results chosen from the performed measurements for both steam generators are gathered in Tab. 1. The table contains only the most important inlet and outlet parameters from three measurement series. Series A1** and A1 are one and the same measurement that differs in steam mass flow rate. In the first case, $\dot{m}_{steam,IV}$ has been calculated on the basis of water gauge reading. In the latter case, however, the steam mass flow rate results from the heater power. These two values are very similar, but the first one is burdened with a higher uncertainty. Measurements B1 and B2 were carried out on a high-powered steam generator with the use of two different fan gears. In both cases ambient conditions were close to each other. Steam mass flow rate was derived from the heater power and the condensate flow rates were provided by the energy and moisture balances.

Relative humidity φ_{II} in all cases is low and varies from 21% to 33% despite the significant difference in the obtained condensate. This situation occurs due to the temperature ranging from 38 °C to over 63 °C. Such low values of the relative humidity suggest that the air is far from saturation.

Table 2 contains measured data of all three combi-steamer operating

modes. Each of them has been examined on both fan gears. Values of the condensate mass flow rate were measured and used in steam flow rate determination.

Table 2: Combi-steamer – measurements.

Symbol	C1	C1	C2	C2	C3	C3	C4	C4	C5	C5
t_I, °C	25.4	26.5	26.1	27.2	26.4	25.5	26.4	27.0	27.0	25.5
φ_I, %	29	31	29	30	28	26	32	29	29	21
$p_I{}^*$, kPa	100.23	100.77	99.94	99.84	100.72	100.23	100.23	100.23	100.07	100.08
t_{II}, °C	31.9	32.8	42.5	42.4	42.4	42.3	50.2	46.7	49.4	46.5
φ_{II}, %	21	22	14	14	14	13	12	14	10	9
$\dot{m}_{steam,IV}$, g/s	0.23	0.19	0.73	0.71	0.83	1.06	1.27	1.56	0.96	1.11
$\dot{m}_{cond,III}$, g/s	0.18	0.15	0.53	0.54	0.60	0.74	0.73	0.97	0.81	0.73
Gear	1	2	1	2	1	2	1	2	1	2

*reference pressure

6 Analysis outcome and discussion

Results of measurements of the condensation hood in cooperation with steam generators are gathered in Tab. 3. Balances inconsistency $\Delta\dot{H}$ was lower than 5%. The condensation efficiency (Eq.(12)) in cases A1 and A2 is about 90% whereas in cases B1 and B2 is significantly lower because a much higher steam flow rate (about 11.50 g/s in case B in comparison to 1.36 g/s in case A). It means that the maximum power output of the heat exchanger was reached – approximately 6.5 kW for gear 1 and over 9 kW for gear 2. In addition, especially in case B2, a significant moisture increase ($\dot{m}_{v,I}$ in comparison to $\dot{m}_{v,II}$) in the air can be noticed. Conclusion is one – not condensed steam is diluted in the output air. However, the condensation hood during normal (casual) work will never have to cope with such heat loads as in case B2.

The combi-steamer output is not exactly known. Any measurements of mass flow rate are difficult and burdened with significant errors due to high temperature (at around 100 °C) and high humidity. Pitot tubes were used but any brief exposure to combi-steamer output resulted in the tube clogging with droplets, which affected measurement results. Situation with the humidity probe was similar. Too high moisture content prevented us

Table 3: Steam generators – results.

Symbol	A1	A2	B1	B2
w_I*	0.0077	0.0084	0.0099	0.0059
$\dot{m}_{v,I}$, g/s	1.61	1.76	1.81	1.31
w_I*	0.0083	0.0091	0.0569	0.0475
$\dot{m}_{v,II}$, g/s	1.73	1.90	10.39	8.66
$\dot{m}_{steam,IV}$, g/s	1.36	1.36	11.49	11.50
$\dot{m}_{cond,III}$, g/s	1.21	1.25	2.91	4.15
$\dot{m}_{cond,III,ad}$, g/s	0.02	-0.02	0.00	0.00
$\Delta\dot{H}$, %	1.54	1.13	2.46	0.24
$\dot{Q}$, kW	2.8	2.8	6.5	9.3
η, %	89.3	91.6	25.3	36.1
Gear	1	1	1	2

*mass of moisture per unit mass of dry air

from using our probes. For this reason any attempt to measure reliably the moisture content and total mass flow rate requires prior separation of moisture from the air. To do so, a dedicated device is necessary. Due to a low gauge pressure (several pascals), the introduction of any additional device causes a relatively significant pressure drop.

Preliminary results showed that only part of the energy balances is closed without any additional actions. An explanation was quite simple – part of the condensate 2.b dripped down the wall of SDF back to the combi-steamer (segment a-c) according to Fig. 5. Those difficulties forced a specific approach compensation of the balances. It required reduction of the balance inconsistency by adjusting the mass flow rate of the condensate and steam. According to Eq. (7), where enthalpies of air and heat losses ($\dot{H}_I$, $\dot{H}_{II}$ and $\dot{Q}_V$, respectively) are properly estimated and fixed by design considerations, the balance inconsistency depends on just two remaining elements – enthalpy of the steam and the condensate ($\dot{H}_{IV}$ and $\dot{H}_{III}$, respectively). Assuming that both of them are correct except for the mass flow rates $\dot{m}_{cond,III}$ (that is deficient) and resulting from that $\dot{m}_{steam,IV}$ (see Eq. (7)), it becomes justified to compensate the missing condensate by an increase of $\dot{m}_{cond,III}$ by $\dot{m}_{cond,III,ad}$.

To show the effect of balance compensation approach, the final results for Case C have been divided into two tables: Tab. 4 with selected results before and after balance compensation, and Tab. 5 with the results after

Table 4: Combi-steamer chosen balances – compensation.

Symbol	C1*	C1**	C2*	C2**
w_I***	0.0067	0.0067	0.0068	0.0068
$\dot{m}_{v,I}$, g/s	1.49	1.49	1.49	1.49
w_{II}***	0.0068	0.0068	0.0075	0.0075
$\dot{m}_{v,II}$, g/s	1.52	1.52	1.66	1.66
$\dot{m}_{steam,IV}$, g/s	0.19	0.75	0.71	1.70
$\dot{m}_{cond,III}$, g/s	0.15	0.71	0.54	1.53
$\dot{m}_{cond,III,ad}$, g/s	0.00	0.56	0.00	0.99
$\Delta\dot{H}$, %	-11.33	0.03	-16.60	0.05
$\dot{Q}$, kW	0.4	1.4	0.4	1.6
η, %	83.4	95.9	76.7	90.3
Gear	2		2	

*results before balance compensation
**results after balance compensation
***mass of moisture per unit mass of dry air

compensation only.

Table 4 contains two chosen measurement series before and after balance compensation procedure described above. A high energy balance inconsistency $\triangle\dot{H}$ (over ten percent) has been greatly reduced by simple condensate flow rate compensation (not captured condensate $\dot{m}_{cond,III,ad}$). A significant amount of the condensate was missing – approximately 70%. Moreover, the missing condensate affects the condensation efficiency (Eq. (12)) that increases from 83% in Case C1 and from 76% in Case C2 by over 10% to over 90% in both cases. While the missing condensate $\dot{m}_{cond,III,ad}$ is included in $\dot{m}_{cond,III}$, the steam flow $\dot{m}_{steam,IV}$ is affected as well. Because of that, share of the condensed steam in the overall steam flow rate increases, which translates directly onto the higher condensation efficiency.

Results after balance compensation (condensation hood in cooperation with the combi-steamer) are shown in Tab. 5. All balances inconsistencies are negligible – less than 1%. Steam flow rates differ from 0.65 g/s for case C1 to 2.51 g/s and 2.44 g/s for cases C4 and C5. Compensating condensate flow rates $\dot{m}_{cond,III,ad}$ varies depending on the case: from barely 0.17 g/s in case C4 gear 2 to even 1.28 g/s in the same case but with gear 1. Case C5 gear 2 turned out to be the only one with a higher additional condensate rate – 1.33 g/s.

Table 5: Combi-steamer – results.

Symbol:	C1	C1	C2	C2	C3	C3	C4	C4	C5	C5
$w_I{}^*$	0.0059	0.0067	0.0062	0.0068	0.0059	0.0053	0.0068	0.0065	0.0065	0.0043
$\dot{m}_{v,I}$, g/s	1.12	1.49	1.17	1.49	1.11	1.17	1.28	1.43	1.22	0.97
$w_{II}{}^*$	0.0061	0.0068	0.0073	0.0075	0.0071	0.0067	0.0097	0.0091	0.0074	0.0061
$\dot{m}_{v,II}$, g/s	1.16	1.52	1.37	1.66	1.34	1.49	1.82	2.02	1.37	1.35
$\dot{m}_{steam,IV}$, g/s	0.65	0.75	1.62	1.70	1.61	2.02	2.51	1.73	2.02	2.44
$\dot{m}_{cond,III}$, g/s	0.60	0.71	1.42	1.53	1.38	1.70	2.01	1.76	1.87	2.06
$\dot{m}_{cond,III,ad}$, g/s	0.42	0.56	0.89	0.99	0.78	0.96	1.28	0.96	1.06	1.33
$\Delta\dot{H}$, %	0.08	0.03	-0.05	0.05	-0.07	-0.01	-0.07	-0.11	0.02	0.01
$\dot{Q}$, kW	1.4	1.6	3.2	3.5	3.1	3.8	4.5	4.0	4.2	4.6
η, %	93.2	95.3	87.7	90.3	86.0	84.2	78.9	75.0	92.4	84.4
Gear:	1	2	1	2	1	2	1	2	1	2

*mass of moisture per unit mass of dry air

Compensating condensate (the missing condensate) constitutes a significant part of the overall condensate that allows for closing the energy balance and, approximately, equals to 59%. In other words – during measurements with the combi-steamer about 2/3 of the condensate was not captured. With the use of SDF we proved that some amount of the condensate dripped down back to the combi-steamer instead of the condensate container according to Fig. 5. This was a surprise, because the shape of SDF should prevent this from happening. The condensation efficiency, again, is related to the steam and condensate flow rates. Cases C1 and C2 are characterized by the highest efficiency (of about 90%), whereas the remaining cases have a noticeably lower efficiency. The results obtained for Cases C4 and C5 are surprising. In both cases, condensation efficiencies are slightly lower for gear 2. Moreover, steam flows as well as condensation flows are not consistent. This is difficult to explain, especially since experiments with the steam generator carried out in a similar manner produced more accurate results. However, it can be explained, at least in part, by the combi-steamer complexity and a difficulty to determine its way of work. In addition to that, measurement errors could contribute to this.

7 Summary and conclusions

In this work a numerous measurements of the condensation hood have been carried out in different conditions. At first, the condensation hood in cooperation with the steam generator (3.4 kW) was investigated in conditions similar to its normal working conditions (about 1.4 g/s of steam). Then, an extreme case has been taken into account to achieve the maximum heat power of the device – 27 kW steam generator – with a use of both fan gears allowed. The steam flow rate supplying the condensation hood obtained in this case amounts to 11.5 g/s. The steam flow rate was derived from the electric heater power and enthalpy of evaporation.

In the next step, cooperation with dedicated combi-steamer was tested and all available oven's operating modes have been investigated on both available fan gears. However, the steam flow rate was not possible to be measured reliably due to a high moisture content affecting available measurement instruments, high pressure-drop sensitiveness of the oven and semi-stationary work of the heater. The condensate flow rate turned out to be difficult to catch as well. The use of SDF did not meet the expectations and still significant part of the condensate flowed back to the oven.

The mathematical model of the condensation hood has been developed in order to assess performed measurements and to carry out a preliminary diagnosis. This model consists of three balances of air, moisture and energy. The obtained energy balances inconsistencies were high (of a dozen or so percent) and needed to be compensated. Unfortunately, due to lack of reliable information concerning steam and condensate flow rates (the number of unknowns is higher than the number of equations), the application of widely-known standard data reconciliation methods was not possible. Thus, the mathematical model was used to determine the missing condensate and/or steam flows.

This approach affected results of the steam and condensate flow rates, condensation efficiency, heat power of the heat exchanger and balance inconsistencies. The obtained values of steam flow vary depending on the oven's operating mode from 0.65 g/s for case C1 to 2.55 for case C4. Not much less demanding was case C5, which differs from C4 only by an operating parameter HP value. The condensate flow rate differs in similar way. In case C1 (where steam flow was the lowest) the obtained condensate flow rate is the lowest as well and equals to 0.71 g/s, whereas the highest condensate flow rate of 2.06 g/s obtained in case C5.

Steam generators (Case A and Case B) were used as a benchmark in re-

fining measurement methodology and developing the mathematical model. Results were very satisfactory. Balances inconsistencies did not exceed 3% so any further condensate compensation was not necessary. In the case of a combi-steamer (Case C), however, all energy balance inconsistencies were much higher (from approximately 15% to over 25%). After the compensation the differences decreased and eventually they do not exceed 1%.

The heat power of the heat exchanger (resulting directly from the condensed steam) varies from 1.34 kW in case C1 gear 1 through 4.64 (case C5 gear 2) to 9.34 kW in case B2.

Calculations show that the highest condensation efficiency of almost 96% was reached in a less heat demanding case C2, while the lowest efficiency (75%) was obtained in one of the most demanding cases – case C4. In separate case B1 the efficiency decreased to 25%, but it was an extreme case just to investigate the condensation hood performance under the most unfavorable conditions (maximum steam input, lowest fan gear 1).

The experiments proved that the steam channel 6 showed in Fig. 1 is not sufficiently wide, therefore the majority of steam stays in bundle 2. This leads directly to the situation, where pipes of bundle 2 are heavily loaded, while pipes of bundle 3 are hardly loaded. Hence, the potential of the heat exchanger is not fully used.

The condensation efficiency of the condensation hood is very high and it can be concluded that the device performs well. However, a detailed analysis of this device is not possible through the analytical model only. Thus a numerical model needs to be developed. The numerical study of the considered device is a subject of further study.

The results prove that the approach presented in this paper was justified and gave a reasonable values. It also allowed us to assess the quality of measurements. Thus, the obtained results can be used in the next step – validation of a numerical model.

Acknowledgements Financial assistance was provided by grant no. POIR.03.02.01-18-0019/15-00 funded by the Polish Agency for Enterprise Development, Poland, and is here acknowledged.

Received 4 July 2019

References

[1] Diane Lane: ONE FOR ALL. Caterer & Hotelkeeper, **203**(2013), 4799, 56–58.

[2] Henny Penny Corp. Combi cooking. 2007.

[3] Su J., Sun Z., Zhang D: *Numerical analysis of steam condensation over a vertical surface in presence of air.* Ann. Nucl. Energy **72**(2014), 10, 268–276.

[4] Fan G., Tong P., Sun Z., Chen Y.: *Development of a new empirical correlation for steam condensation rates in the presence of air outside vertical smooth tube.* Ann. Nucl. Energy **113**(2018), 3, 139–146.

[5] Noori Rahim Abadi S.M.A., Mehrabi M., Meyer J.P.: *Numerical study of steam condensation inside a long, inclined, smooth tube at different saturation temperatures.* Int. J. Heat Mass Trans. **126**(2018), 11, 15–25.

[6] Bian H., Sun Z., Cheng X., Zhang N., Meng Z., Ding M.: *CFD evaluations on bundle effects for steam condensation in the presence of air under natural convection conditions.* In. Commun. Heat. Mass **98**(2018),11, 200–208.

[7] O'Donovan A., Grimes R.: *Pressure drop analysis of steam condensation in air-cooled circular tube bundles.* Appl. Therm. Eng. **87**(2015), 8, 106–116.

[8] Tarasov G.I., Bol'shukhin M.A., Sinitsyn A.N., VasyatkinA. G., Kustov S.V.: *Experimental studies of heat transfer during steam condensation on a vertical multirow on-line bundle of slightly inclined coil tubes with and without noncondensable gas in the bundle.* Therm. Eng. **59**(2012), 1, 26–32.

[9] Fan G., Tong P., Sun Z., Chen Y.: *Experimental study of pure steam and steam–air condensation over a vertical corrugated tube.* Prog. Nucl. Energ. **109**(2018), 11, 239–249.

[10] Wais P.: *Fluid flow consideration in fin-tube heat exchanger optimization.* Arch. Thermodyn. **31**(2010), 3, 87–104.

[11] Tian L., He Y., Tao Y., Tao W.: *A comparative study on the air-side performance of wavy fin-and-tube heat exchanger with punched delta winglets in staggered and in-line arrangements.* Int. J. Therm. Sci. **48**(2009), 9, 1765–1776.

[12] Kennedy I.J., Spence S.W.T., Spratt G.R., Early J.M.: *Investigation of heat exchanger inclination in forced-draught air-cooled heat exchangers.* Appl. Therm. Eng. **54**(2013), 2, 413–421.

[13] Lee D.H., Jung J.M., Ha J.H., Cho Y.I.: *Improvement of heat transfer with perforated circular holes in finned tubes of air-cooled heat exchanger.* Int. Commun. Heat Mass **39**(2012), 2, 161–166 .

[14] Kashani A.H.A., Maddahi A., Hajabdollahi H.: *Thermal-economic optimization of an air-cooled heat exchanger unit.* Appl. Thermal Eng. **54**(2013), 1, 43–55.

[15] Cengel Y.A.: *Heat Transfer: A Practical Approach (3rd Edn.).* McGraw-Hill, Boston 2007.

[16] Wang Y., Zhao Q., Zhou Q., Kang Z., Tao W.: *Experimental and numerical studies on actual flue gas condensation heat transfer in a left–right symmetric internally finned tube.* Int. J. Heat Mass Tran. **64**(2013), 9, 10–20.

[17] Mohapatra K., Mishra D.: *Effect of fin and tube configuration on heat transfer of an internally finned tube.* Int. J. Numer. Meth. Heat Fluid Fl. **25**(2015), 8, 1978–1999.

[18] Wang Q.-W., Lin M., Zeng M.: *Effect of lateral fin profiles on turbulent flow and heat transfer performance of internally finned tubes.* Appl. Therm. Eng. **29**(2009), 14-15, 3006–3013.

[19] Kim D.-K.: *Thermal optimization of internally finned tube with variable fin thickness.* Appl. Therm. Eng. **102**(2016), 6, 1250–1261.

[20] Huq M., Huq A.M. Aziz-ul, Rahman M.M.: *Experimental measurements of heat transfer in an internally finned tube.* Int. Commun. Heat Mass **25**(1998), 5, 619–630.

[21] Taler D.: *Model matematyczny oraz badania aerodynamiczne i przepływowo-cieplne chłodnicy samochodowej.* Archiwum Motoryzacji **4**(2001), 145–162 (in Polish).

[22] Long Y., Wang S., Wang J., Zhang T.: *Mathematical model of heat transfer for a finned tube cross-flow heat exchanger with ice slurry as cooling medium.* Procedia Engineer. **146**(2016), 1, 513– 522.

[23] Li B., You S., Ye T., Zhang H., Li X., Li C.: *Mathematical modeling and experimental verification of vacuum glazed transpired solar collector with slit-like perforations.* Renew. Energ. **69**(2014), 9, 43–49.

[24] El Mansouri A., Hasnaoui M., Amahmid A., Dahani Y.: *Transient theoretical model for the assessment of three heat exchanger designs in a large-scale salt gradient solar pond: Energy and exergy analysis.* Energ. Convers. Manage. **167**(2018), 7, 45–62.

[25] Klopfenstein R. Jr.: *Air velocity and flow measurement using a Pitot tube.* ISA Transactions **37**(1998), 4, 257–2639.

[26] Sun Z., Li Z., Zheng J.: *Influence of improper installation on measurement performance of Pitot tube.* In: Proc. 2009 Int. Conf. on Industrial Mechatronics and Automation. IEEE, **5**(2009), 53–56.

[27] Narasimhan S., Narasimhan S.: *Data reconciliation using uncertain models.* Int. J. Adv. Eng. Sci. Appl. Math. **4**(2012),(1-2), 3–9.

[28] Mandel D., Abdollahzadeh A., Maquin D., Ragot J.: *Data reconciliation by inequality balance equilibration: a LMI approach.* Int. J. Miner. Proces. **53**(1998),3, 157–169.

[29] Narasimhan S., Shah S.L.: *Model identification and error covariance matrix estimation from noisy data using PCA.* Control Eng. Pract. **16**(2008), 1, 146–155.

[30] *ASHRAE Handbook – Fundamentals.* Refrigerating American Society of Heating and Air-Conditioning Engineers. Atlanta 2001.